Atmospheric Circulation Cells Associated with the El Niño–Southern Oscillation

CHUNZAI WANG

Physical Oceanography Division, NOAA Atlantic Oceanographic and Meteorological Laboratory, Miami, Florida

(Manuscript received 20 February 2001, in final form 10 July 2001)

ABSTRACT

Atmospheric circulation cells associated with the El Niño–Southern Oscillation (ENSO) are described and examined using the NCEP–NCAR reanalysis field and the NCEP sea surface temperature (SST) from January 1950 to December 1999. The divergent wind and pressure vertical velocity are employed for the identification of atmospheric circulation cells. The warm phase of ENSO shows positive SST anomalies in the equatorial eastern Pacific and along the east coast of Asia and the west coast of North America, and negative SST anomalies in the off-equatorial western Pacific and in the central North Pacific. Associated with this SST anomaly distribution are variations of atmospheric zonal and meridional circulation cells over the Pacific. The equatorial zonal Walker circulation cell is weakened, consistent with previous schematic diagrams. The anomalous meridional Hadley circulation cell in the eastern Pacific shows the air rising in the Tropics, flowing poleward in the upper troposphere, sinking in the subtropics, and returning back to the Tropics in the lower troposphere. The anomalous Hadley cell in the western Pacific is opposite to that in the eastern Pacific. The divergent wind and vertical velocity also show a midlatitude zonal cell (MZC) over the North Pacific. The mean MZC is characterized by the air rising in the central North Pacific, flowing westward and eastward in the upper troposphere, descending in the east coast of Asia and the west coast of North America, then returning back to the central North Pacific in the lower troposphere. The anomalous MZC during the mature phase of El Niño shows an opposite rotation to the mean MZC, indicating a weakening of the MZC.

1. Introduction

In a seminal paper, Bjerknes (1969) postulated an atmospheric circulation cell in the zonal-vertical plane over the equatorial Pacific, which he named the ''Walker circulation'' since this circulation is part of the global Southern Oscillation phenomenon defined earlier by Sir Gilbert Walker (1923, 1924, 1928). The Walker circulation cell is characterized as the air ascending in the equatorial western Pacific, flowing eastward in the upper troposphere, sinking in the equatorial eastern Pacific, and returning toward the equatorial western Pacific in the lower troposphere. Bjerknes also visualized a close relation among the Southern Oscillation, east–west sea surface temperature (SST) contrast in the equatorial Pacific Ocean, and the thermally driven Walker cell. Since then, the zonal Walker circulation cell has been recognized to be associated with the interannual phenomenon of the El Niño–Southern Oscillation (ENSO) that has been intensively studied (e.g., Philander 1990; McCreary and Anderson 1991; Neelin et al. 1998). Schematic diagrams of the Walker circulation cell during ENSO are well known (e.g., Webster and Chang 1988; McPhaden et al. 1998). However, how the Walker circulation cell evolves during ENSO from data has not been well studied, probably because of a lack of observational data. The Walker circulation cell associated with ENSO has been shown little quantitatively.

The atmosphere also has meridional circulation cells: the Hadley cell and the Ferrel cell (e.g., Trenberth et al. 2000; and references therein). The Hadley circulation cell is also thermally driven, located in the tropical and subtropical regions. The heated tropical air rises and flows aloft toward the subtropical region where it cools, sinks, and flows back to the tropical region. The Ferrel cell is an extratropical meridional circulation cell characterized by the air ascending in the extratropical region and descending in the subtropical region. Unlike the Walker and Hadley cells, the Ferrel cell is a thermally indirect cell. The Ferrel cell is forced mostly by transient baroclinic eddy activity through associated poleward heat and momentum transports (e.g., Holton 1992). Little is known about how these atmospheric meridional cells vary during the evolution of ENSO. Also, a strong zonal wind speed core, called the ''jet stream,'' is located just below the tropopause in the extratropics. Previous studies (e.g., Horel and Wallace 1981) suggested that ENSO teleconnections link the jet stream with ENSO.

Corresponding author address: Dr. Chunzai Wang, Physical Oceanography Division, NOAA Atlantic Oceanographic and Meteorological Laboratory, 4301 Rickenbacker Causeway, Miami, FL 33149.
E-mail: wang@aoml.noaa.gov

The recently available data of the National Centers for Environmental Prediction–National Center for Atmospheric Research (NCEP–NCAR) reanalysis field (Kalnay et al. 1996) provide an opportunity to study the atmospheric circulation patterns associated with ENSO. The present paper uses the NCEP–NCAR reanalysis field and the NCEP SST data (Smith et al. 1996) to describe and investigate how the Walker cell, the Hadley cell, the Ferrel cell, and the jet stream vary during the evolution of ENSO. Additionally, the combination of atmospheric divergent wind and vertical motion data shows an atmospheric zonal cell in the midlatitudes of the North Pacific. The rest of the paper is organized as follows. Section 2 introduces the data used in this paper. Section 3 shows the annual variability of the atmospheric circulation patterns. Sections 4 and 5 show composites and temporal variations of the atmospheric circulation associated with ENSO, respectively. Section 6 provides a discussion and summary.

2. Data

The major data source in this study is the NCEP–NCAR reanalysis field from January 1950 to December 1999. The NCEP–NCAR reanalysis field uses a state-of-the-art global data assimilation system on a 2.5° lat $\times$ 2.5° long grid (see Kalnay et al. 1996 for details). Variables used in this study are monthly atmospheric horizontal wind velocity, vertical velocity, and velocity potential at levels of 1000, 925, 850, 700, 600, 500, 400, 300, 250, 200, 150, and 100 mb. The vertical component of wind field in the NCEP–NCAR reanalysis field is pressure vertical velocity. In our presentation, we multiply the pressure vertical velocity by -1, so positive values of the vertical velocity indicate an upward movement of air parcels. Since we are interested in tropical atmospheric circulation and northern midlatitude atmospheric circulation associated with the Pacific ENSO, the analyses in this paper are shown from 20°S–60°N to 100°E–80°W. Although our analyses were performed globally, our focus herein is on the Pacific. Results associated with Atlantic climate variability are reported in a companion paper (Wang 2002, manuscript submitted to *J. Climate*).

Horizontal wind velocity can be divided into a nondivergent (or rotational) part and a divergent (or irrotational) part (e.g., Mancuso 1967; Krishnamurti 1971; Krishnamurti et al. 1973): $\mathbf{v} = \mathbf{v}_\psi + \mathbf{v}_\phi = \mathbf{k} \times \nabla\psi + \nabla\phi$, where ψ is streamfunction and ϕ is velocity potential. The first part does not contribute to atmospheric divergent fields associated with atmospheric vertical motion (it is nondivergent). It is well known that the Walker and Hadley cells are thermally driven, associated with atmospheric convergence–divergence. Atmospheric heating associated with convection induces atmospheric convergence–divergence that drives atmospheric vertical motion and circulation. Therefore, what it matters to atmospheric cells associated with atmospheric convergence–divergence is the divergent part of the wind although the rotational part is usually larger. In the search for evidence of atmospheric circulation cells, it is essential not only to isolate the divergent part of the wind but also to ascertain the continuity following the flow between the centers of upward and downward motion (e.g., Krishnamurti et al. 1973; Hastenrath 2001). The analyses of the divergent wind and vertical motion are prerequisites indispensable for the identification of atmospheric circulation cells. Following these, we will mainly focus on the distributions of atmospheric vertical motion and the divergent component of the wind when we discuss atmospheric circulation cells. Newman et al. (2000) compared the 200-mb wind divergence fields from the NCEP–NCAR, the European Centre for Medium-Range Weather Forecasts (ECMWF), and the National Aeronautics and Space Administration (NASA) reanalyses. Although the details of the divergence fields are different among these analyses, basic patterns are reasonably consistent (also Trenberth et al. 2000).

Monthly SST data are also used in this study. SST data are taken from the NCEP SST data set on a 2° lat $\times$ 2° long grid from January 1950 to December 1999. These SST fields were produced by using a spatial interpolation method employing empirical orthogonal function analysis (see Smith et al. 1996 for the detailed description). With all of these data, we first calculate monthly climatologies based on the full record period (1950–99) and then anomalies are obtained by subtracting the monthly climatologies for each dataset from the data.

3. Annual variability

To better understand anomaly variations of atmospheric circulation cells, we first consider annual variability of tropospheric circulation patterns. Figure 1 shows the boreal winter (January) climatologies of tropospheric circulation. Centers of low (high) velocity potential are associated with divergent outflow (convergent inflow) winds. Figures 1a–c show that divergence (convergence) at the upper troposphere corresponds to convergence (divergence) at the lower troposphere, associated with upward (downward) vertical motion at the midtroposphere (three levels of 200, 500, and 850 mb are chosen as representative of the upper, mid-, and lower troposphere, respectively). Centers of upper-tropospheric divergence and lower-tropospheric convergence in the equatorial region just west of the date line are characterized by strong upward velocity at the midtroposphere with maximum upward velocity in the off-equatorial regions. The equatorial eastern Pacific is associated with upper-tropospheric convergence, lower-tropospheric divergence, and midtropospheric downward vertical motion. All of these are consistent with Pacific climate features of the western Pacific warm pool and the equatorial eastern Pacific cold tongue. Associated with these patterns is the east–west circulation cell

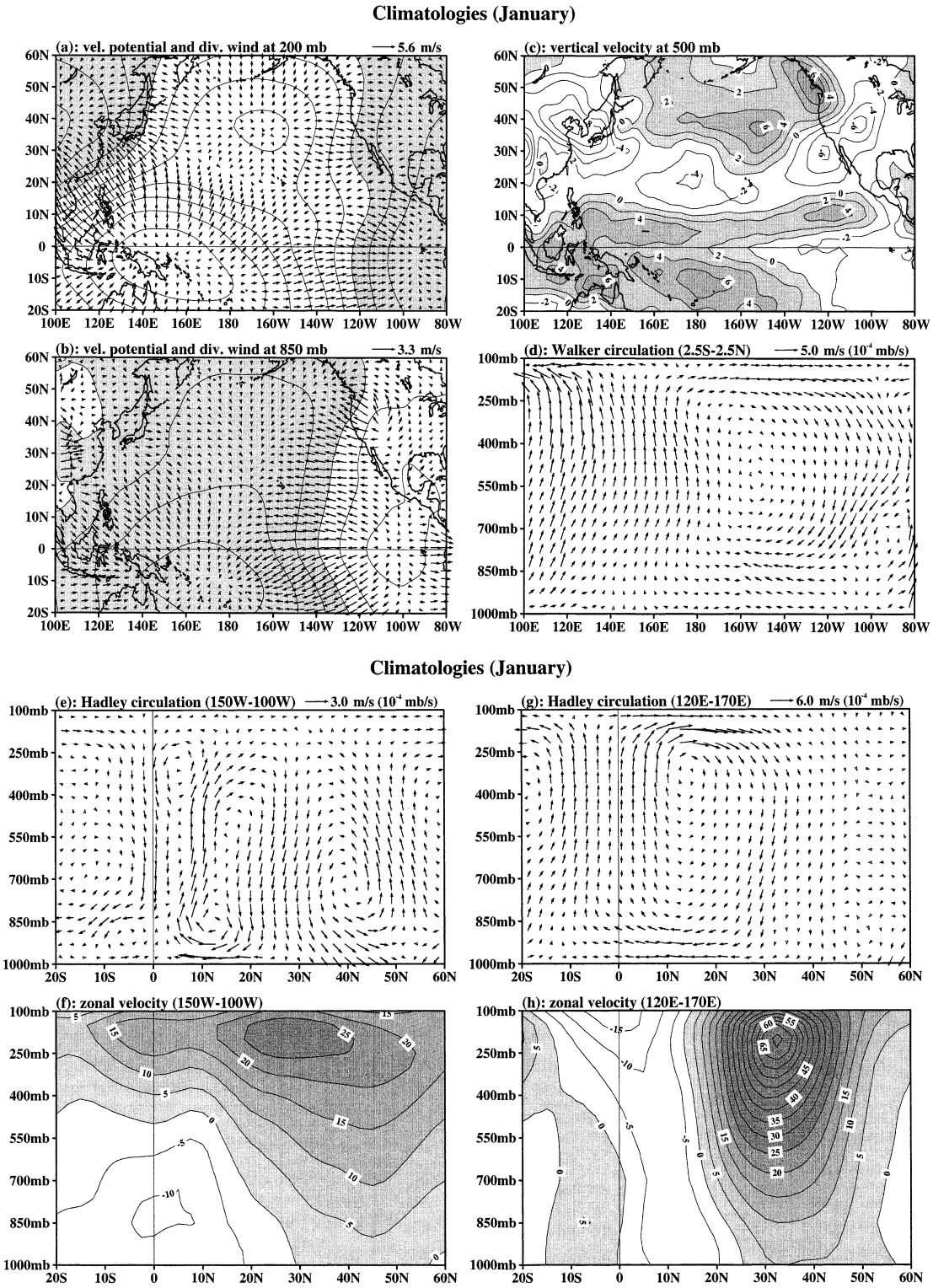

FIG. 1. The boreal winter (Jan) climatologies of tropospheric circulation patterns: (a) 200-mb velocity potential (10^6 m^2 s^{-1}) and divergent wind (m s^{-1}); (b) 850-mb velocity potential (10^6 m^2 s^{-1}) and divergent wind (m s^{-1}); (c) 500-mb vertical velocity (10^{-4} mb s^{-1}); (d) zonal-vertical circulation by averaging divergent wind and vertical velocity between 2.5°S and 2.5°N; (e) meridional-vertical circulation in the eastern Pacific by averaging divergent wind and vertical velocity between 150° and 100°W; (f) total zonal wind in the eastern Pacific between 150° and 100°W; (g) meridional-vertical circulation in the western Pacific by averaging divergent wind and vertical velocity between 120° and 170°E; (h) total zonal wind in the western Pacific between 120° and 170°E. The vertical velocity is taken the negative of the pressure vertical velocity in the reanalysis, i.e., positive values indicate an upward movement of air parcels. Positive values are shaded.

along the equator—the Walker circulation cell, as shown in Fig. 1d. The air ascends in the west, flows eastward in the upper troposphere, sinks in the east, and returns toward the west in the lower troposphere. Figure 1c also clearly shows manifestation of the intertropical convergence zone (ITCZ) in the eastern Pacific around 10°N, with a narrow band of upward vertical motion in the midtroposphere. The South Pacific convergence zone is also indicated around 10°S near the date line. In the midlatitude, Fig. 1c shows upward vertical motion in the central North Pacific and in the west coast of Canada, and downward motion in the east of Asia and in the west of the United States. An east–west band of downward motion in the midtroposphere along 20°N manifests the subtropical high.

As suggested by Figs. 1a–c, the meridional circulation in the western Pacific is different from that in the eastern Pacific. Thus, we separately plot meridional-vertical circulations in the east (150°–100°W) and in the west (120°–170°E) as shown in Figs. 1e–h. In the east, the tropical circulation has two meridional cells with moist air rising in the ITCZ (Trenberth et al. 2000), then diverging northward and southward in the upper troposphere, and descending over the regions to the subtropical high and the equatorial eastern Pacific cold tongue (Fig. 1e). Thus, associated with the south Hadley cell, vertical motion near the equator in the eastern Pacific is downward. The extratropics of the Northern Hemisphere (NH) shows the classic Ferrel cell, with upward motion in the high latitudes and downward motion in the midlatitudes. In the west, a single Hadley cell is shown up, with the air rising in the tropical region, flowing poleward in the upper troposphere in both hemispheres, and returning to the Tropics in the lower northern troposphere (Fig. 1g). The Ferrel cell is relatively weak in the NH midlatitudes of the western Pacific. Total zonal wind shows a core of maximum westerly wind (the jet stream) just below the tropopause around 200 mb in both the eastern and western Pacific (Figs. 1f and 1h). The jet stream in the eastern Pacific, being extended from the midlatitudes to the equatorial region, is much weaker than the one in the western Pacific. The lower troposphere of the equatorial eastern Pacific shows easterly wind, whereas westerly wind appears south of the equator in the western Pacific.

The boreal summer (July) climatologies of tropospheric circulation are shown in Fig. 2. During that time, the centers of upper-tropospheric divergence and lower-tropospheric convergence in the western Pacific shift to the NH. Corresponding to the northward shift of the convergence–divergence centers in the western Pacific is upward motion covered from the equatorial to the northwestern Pacific. The zonal Walker circulation cell becomes well organized in the boreal summer (Fig. 2d).

Associated with the northward shifts during the boreal summer, the meridional cells seem to also have a northward shift. In the eastern Pacific, the Ferrel cell is located at higher latitudes compared with the boreal winter (Figs. 1e and 2e). In the western Pacific, maximum upward motion associated with the Hadley cell has moved to the NH from the Southern Hemisphere (SH), consistent with the northward shift of convergence–divergence centers shown in Figs. 2a and 2b. Both the eastern and western Pacific show cross-equatorial flows from the SH to the NH at the surface. Figures 2f and 2h show that tropical easterly wind extends from the lower to upper troposphere. The jet stream weakens and moves northward during the boreal summer.

The lower- and upper-tropospheric divergent wind fields and the midtropospheric vertical velocity in Figs. 1 and 2 suggest a midlatitude zonal cell (MZC). Based on Figs. 1 and 2, we plot circulation features of zonal-vertical section between 37.5° and 42.5°N (a combination of divergent wind and vertical velocity, similar to the Walker and Hadley cells). The results for January and July are shown in Figs. 3a and 3b, respectively. During the boreal winter, the MZC shows that the air rises in the central North Pacific, diverges eastward and westward in the upper troposphere, descends over regions of the west coast of North America and the east coast of Asia, then flows back to the central North Pacific in the lower troposphere. In the boreal summer, the MZC extends westward and the descending motion branch of the MZC over the east coast of Asia disappears. The MZC shows upward motion in the central Pacific and the east coast of Asia, and downward motion in the west coast of North America.

4. Composites of anomalous circulation cells

During 1950–99, there are seven significant El Niño events (1957/58, 1965/66, 1972/73, 1982/83, 1986/87, 1991/92, and 1997/98) for which the SST anomalies in the Niño-3 region (5°S–5°N, 150°–90°W) exceed 1°C (Fig. 4). The maximum Niño-3 SST anomalies for each warm event occur during the calendar months from November to January except for the 1986/87 event that has double peaks with the major one in the boreal summer. This indicates a robust tendency for mature phase of El Niño to occur toward the end of the calendar year (e.g., Rasmusson and Carpenter 1982). Because of this ENSO phase locking to the seasonal cycle, it is useful and meaningful to derive a composite for better understanding of the evolving nature of atmospheric and oceanic variables during different phases of ENSO.

We consider the El Niño pattern evolution over six phases: antecedent (August–October of year −1), onset (November of year −1–January of year 0), development (March–May of year 0), transition (July–September of year 0), mature (November of year 0–January year +1), and decay (March–May of year +1). Note that year 0 refers to the El Niño year, and year −1 and year +1 refer to the previous and subsequent years of the El Niño year, respectively. Rasmusson and Carpenter (1982) defined the first five phases, and considered the time span from March to May of the El Niño year to

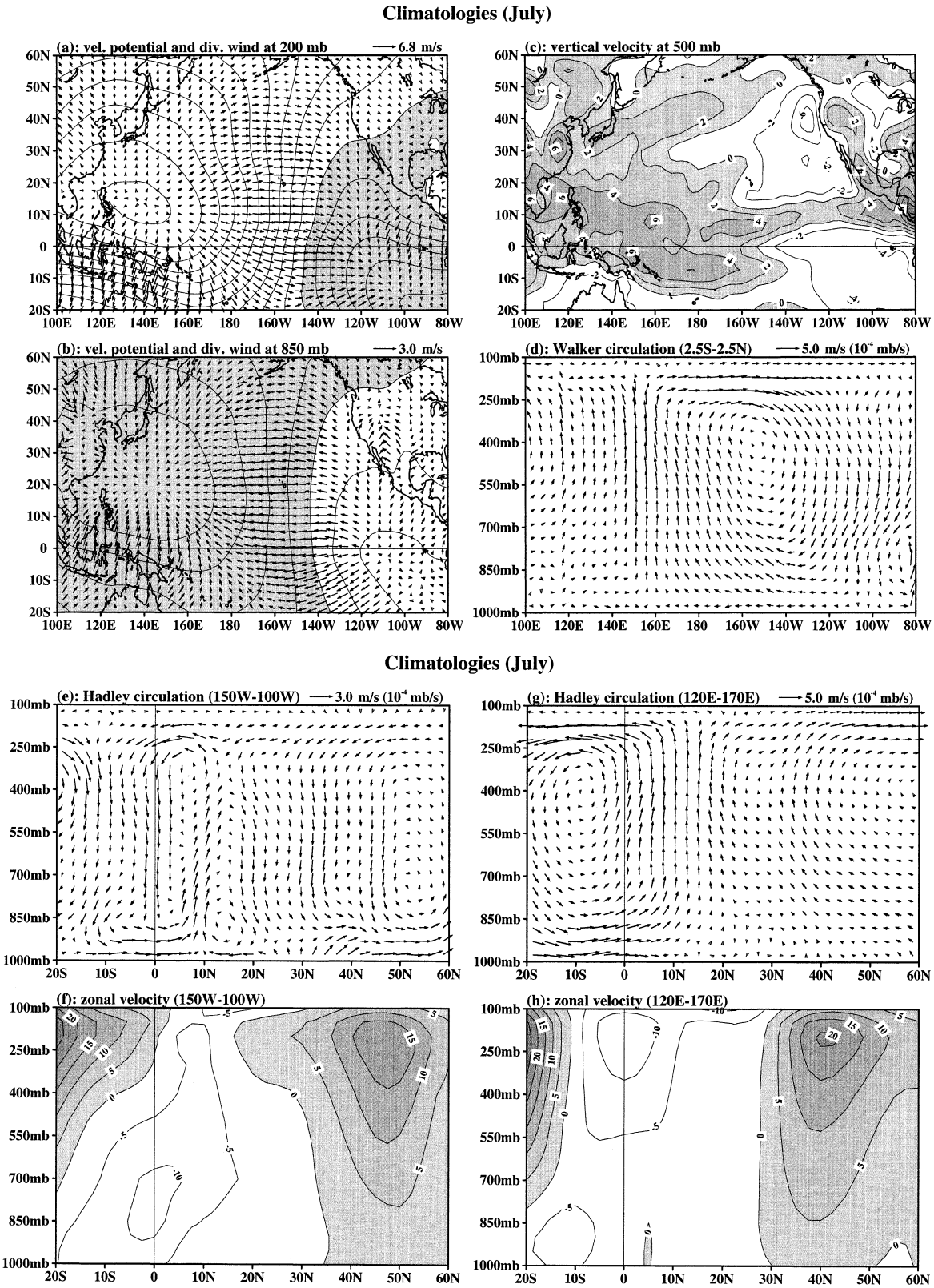

FIG. 2. As in Fig. 1, but for the boreal summer (Jul).

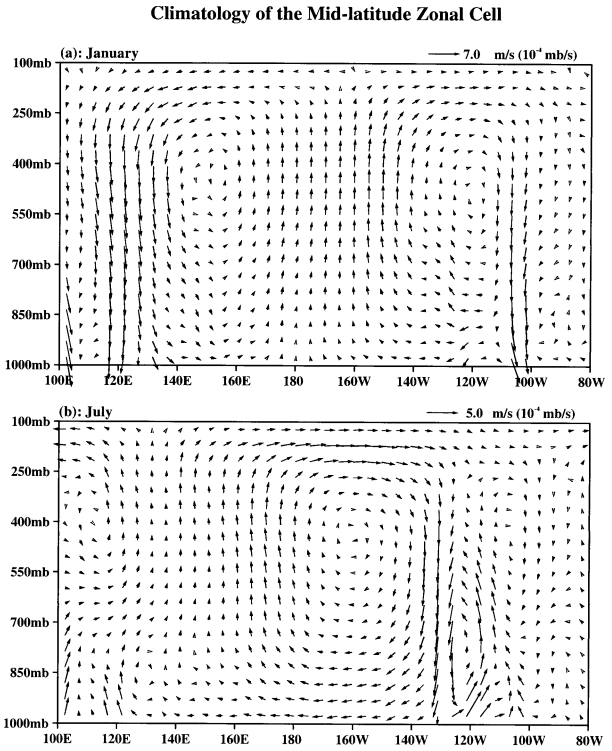

FIG. 3. Climatologies of the MZC in (a) the boreal winter (Jan) and (b) the boreal summer (Jul). The divergent wind and vertical velocity are averaged between 37.5° and 42.5°N.

be the ''peak phase'' because the South American coast reached its peak warming during that period for the El Niño events between 1949 and 1976. However, the El Niño events evolve differently after 1977 (e.g., Wang 1995; Trenberth and Stepaniak 2001). The coastal warmings for the El Niño events between 1977 and 1992 occur in the boreal spring subsequent to the El Niño year rather than in the boreal spring of the El Niño year (Wang 1995). The 1997/98 El Niño develops in both the central Pacific and the South American coast during the spring of 1997 (Wang and Weisberg 2000). In view of these changes, the peak phase of Rasmusson and Carpenter (1982) is changed to the development phase (also in Wang 1995, and Wang and Weisberg 2000). In fact, the Niño-3 SST anomaly index shows that March–May of the El Niño year is a development stage of El Niño (Fig. 4). The decay phase is also added for showing the atmospheric circulation cells during the time of El Niño termination. With these definitions, the SST anomalies for six different phases of El Niño are shown in Fig. 5 and the atmospheric circulation anomaly patterns for different phases are shown in Figs. 6–11. In the composite calculations, we have excluded the 1986/87 El Niño since its phase evolution with respect to the seasonal cycle is at odds with all others.

The antecedent phase exhibits La Niña conditions (Fig. 5a). Observed are cold SST anomalies in the equatorial eastern and central Pacific, warm SST anomalies in the tropical western Pacific, and warm SST anomalies in the central North Pacific. The atmospheric circulation anomalies in Fig. 6 show that centers of upper-tropospheric convergent inflow and of lower-tropospheric divergent outflow are located in the tropical eastern Pacific, associated with anomalous descending motion in the midtroposphere. Upper-tropospheric anomalous divergent outflow, lower-tropospheric anomalous convergent inflow, and midtropospheric anomalous ascending motion are in the far tropical western Pacific. Correspondingly, the Walker circulation shows the air anomalously ascending in the far equatorial western Pacific, flowing eastward aloft, and descending in the equatorial eastern Pacific. The anomalous meridional circulation in the eastern Pacific shows two cells: the Hadley cell and the Ferrel cell. The Hadley cell is characterized by a strong downward motion in the tropical Pacific, whereas the Ferrel cell shows ascending motion in the North Pacific (Fig. 6e). The anomalous Hadley circulation in the western Pacific displays a strong upward motion in the tropical South Pacific (Fig. 6g). During that time, the tropical upper troposphere in both the eastern and western Pacific shows zonal westerly wind anomalies, whereas the tropical lower troposphere exhibits zonal easterly wind anomalies (Figs. 6f and 6h).

During the onset phase (Fig. 5b), the tropical Pacific still remains with cold SST anomalies over the equatorial eastern and central Pacific and weakly warm SST anomalies in the western Pacific, while the central North Pacific shows intensification and eastward extension of warm SST anomalies. Associated with these SST patterns are lower- (upper) tropospheric divergent outflow (convergent inflow) in the equatorial eastern Pacific, lower- (upper) tropospheric convergent inflow (divergent outflow) in the far equatorial western Pacific, and lower- (upper) tropospheric convergent inflow (divergent outflow) around 25°N, 160°W (Figs. 7a and 7b). The Walker circulation shows a strong anomalous subsidence in the equatorial eastern and central Pacific (Fig. 7d). The anomalous Hadley circulation cells in the eastern Pacific and the western Pacific show descending and ascending motion, respectively, in the Tropics (Figs. 7e and 7g). During the onset phase, both the eastern Pacific and the western Pacific display anomalous descending motion in the midlatitudes (between 30° and 40°N for the eastern Pacific and between 25° and 35°N for the western Pacific). Total zonal winds in the lower troposphere of the western Pacific reverse to westerly anomalies from easterly anomalies of the antecedent phase. These lower-tropospheric westerly anomalies in the tropical western Pacific herald the development of El Niño since they can induce eastward-propagating downwelling Kelvin waves that cause a subsequent warming in the central and eastern Pacific (e.g., Wyrtki 1975; McCreary 1976; Busalacchi and O'Brien 1981; Philander 1981).

El Niño begins to develop after the reversal of the lower-tropospheric wind anomalies in the western Pa-

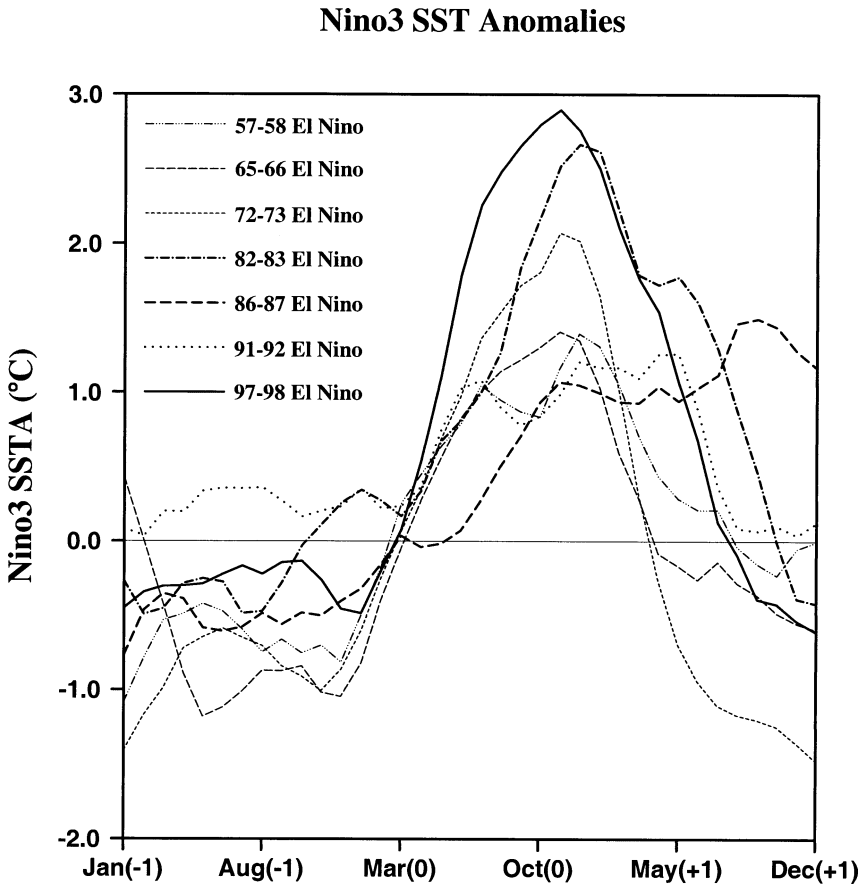

FIG. 4. SST anomalies in the Niño-3 region (5°S–5°N, 150°–90°W) for the seven most significant El Niño events from 1950 to 1999. The numbers −1, 0, and +1 in parentheses represent the previous year of the El Niño year, the El Niño year, and the subsequent year of the El Niño year, respectively.

cific (Fig. 5c). Equatorial warmings occur both in the equatorial central Pacific and in the far eastern Pacific, with large warm SST anomalies in the far eastern Pacific. Cold SST anomalies appear southwest of the North Pacific warm SST anomalies. Corresponding to this development of El Niño are changes of atmospheric circulation patterns. The tropical western Pacific shows lower- (upper) tropospheric anomalous divergent outflow (convergent inflow) and the eastern Pacific exhibits lower- (upper) tropospheric anomalous convergent inflow (divergent outflow). The anomalous Walker circulation cell starts to reverse sign, showing an anomalous ascending motion in the equatorial eastern Pacific (Fig. 8d). During that time, the anomalous Hadley circulation cells in both the eastern and western Pacific also begin to reverse their circulation patterns (Figs. 8e and 8g). The eastern Pacific shows anomalous ascending motion in the equatorial region and in the midlatitude along 30°N, whereas the western Pacific has anomalous descending motion in the equatorial region and in the midlatitude. The lower-tropospheric westerly anomalies in the western Pacific are further developed (Fig. 8h), and lower-tropospheric zonal wind anomalies in the eastern Pacific also reverse to westerly anomalies (Fig. 8f). Upper-tropospheric easterly wind anomalies start to appear in both the western and eastern Pacific during that time (Figs. 8f and 8h).

Following the development and reversal of atmospheric circulation pattern anomalies, the transition phase (Fig. 5d) shows a large-scale warming in the equatorial eastern and central Pacific and cold SST anomalies in the tropical western off-equatorial Pacific. SST anomalies in the central North Pacific have now switched sign from warm to cold. Atmospheric velocity potential anomalies show two centers over the Pacific: one with lower- (upper) tropospheric convergent inflow (divergent outflow) in the equatorial eastern Pacific and the other with lower- (upper) tropospheric divergent outflow (convergent inflow) just to south of the equator in the far western Pacific (Figs. 9a and 9b). Correspondingly, the midtroposphere shows anomalous ascending and descending motions in the equatorial eastern and western Pacific, respectively. The anomalous Walker circulation completely reverses sign from La Niña conditions, with the air rising in the equatorial eastern Pacific, flowing westward aloft, sinking in the equatorial western Pacific,

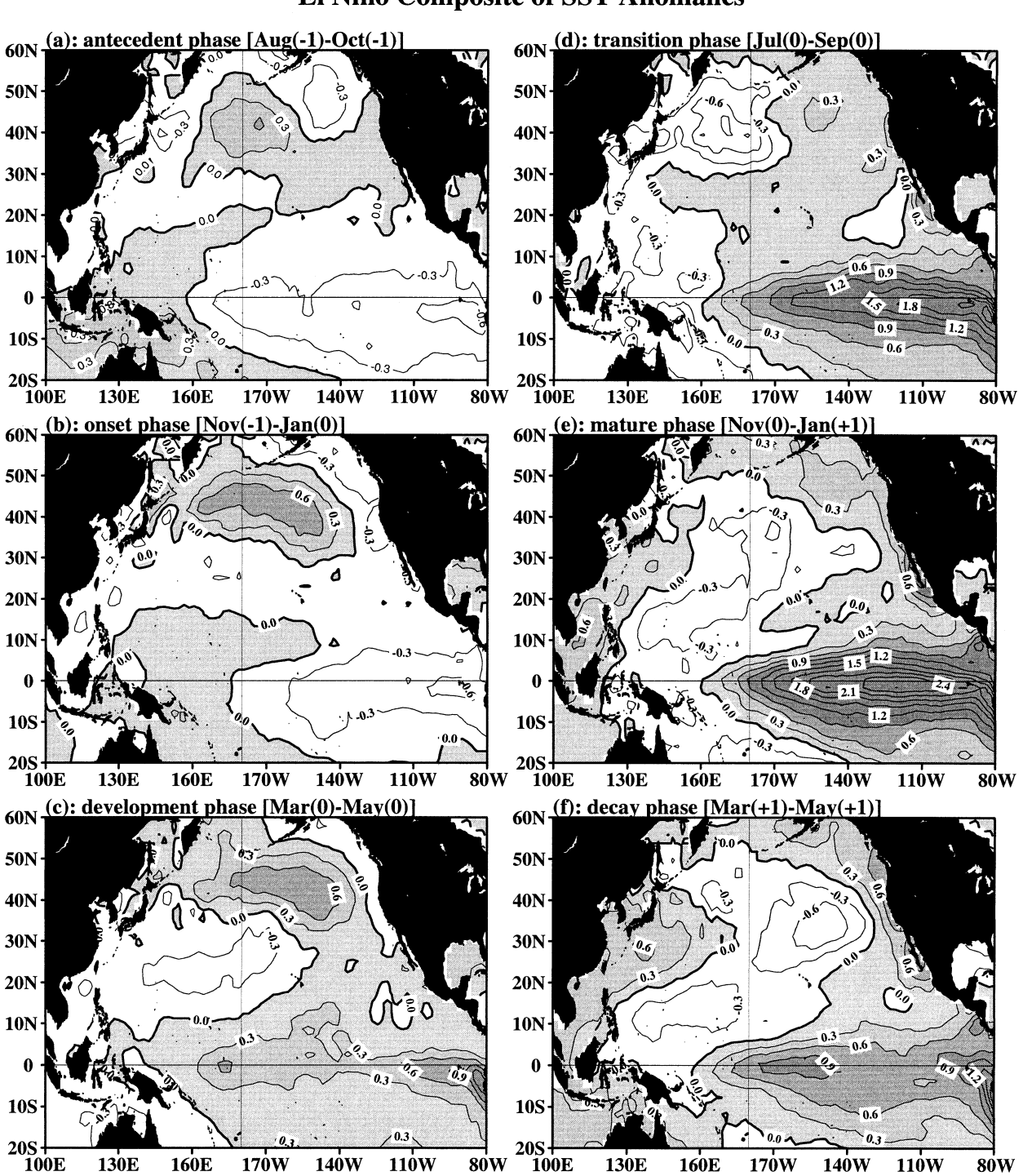

FIG. 5. Pacific SST anomaly composites during (a) the antecedent phase of El Niño, (b) the onset phase of El Niño, (c) the development phase of El Niño, (d) the transition phase of El Niño, (e) the mature phase of El Niño, and (f) the decay phase of El Niño.

and returning back to the eastern Pacific in the lower troposphere. The Hadley circulation in the eastern Pacific shows an anomalous ascending motion near the equator (Fig. 9e), whereas in the western Pacific it displays an anomalous descending motion in the region just south of the equator and an anomalous ascending motion near 10°N (Fig. 9g). During that time, lower-tropospheric westerly wind anomalies in the tropical

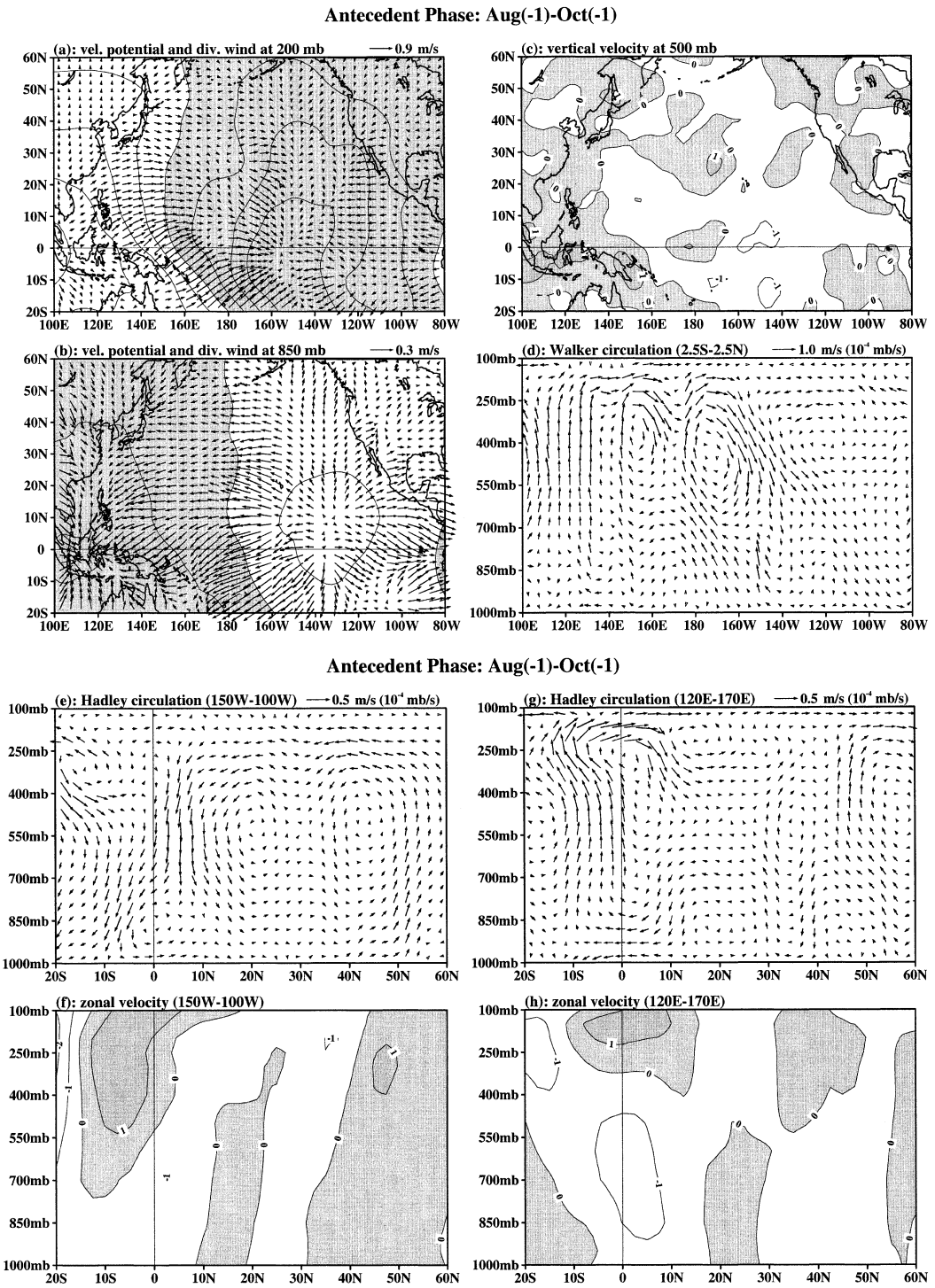

FIG. 6. Atmospheric circulation anomaly composites during the antecedent phase of El Niño. (a) 200-mb velocity potential anomalies (10^6 m^2 s^{-1}) and divergent wind anomalies (m s^{-1}); (b) 850-mb velocity potential anomalies (10^6 m^2 s^{-1}) and divergent wind anomalies (m s^{-1}); (c) 500-mb vertical velocity anomalies (10^{-4} mb s^{-1}); (d) zonal-vertical circulation anomalies by averaging divergent wind and vertical velocity anomalies between 2.5°S and 2.5°N; (e) meridional-vertical circulation anomalies in the eastern Pacific by averaging divergent wind and vertical velocity anomalies between 150° and 100°W; (f) total zonal wind anomalies in the eastern Pacific between 150° and 100°W; (g) meridional-vertical circulation anomalies in the western Pacific by averaging divergent wind and vertical velocity anomalies between 120° and 170°E; (h) total zonal wind anomalies in the western Pacific between 120° and 170°E. The vertical velocity is taken the negative of the pressure vertical velocity in the reanalysis, i.e., positive values indicate an upward movement of air parcels. Positive values are shaded.

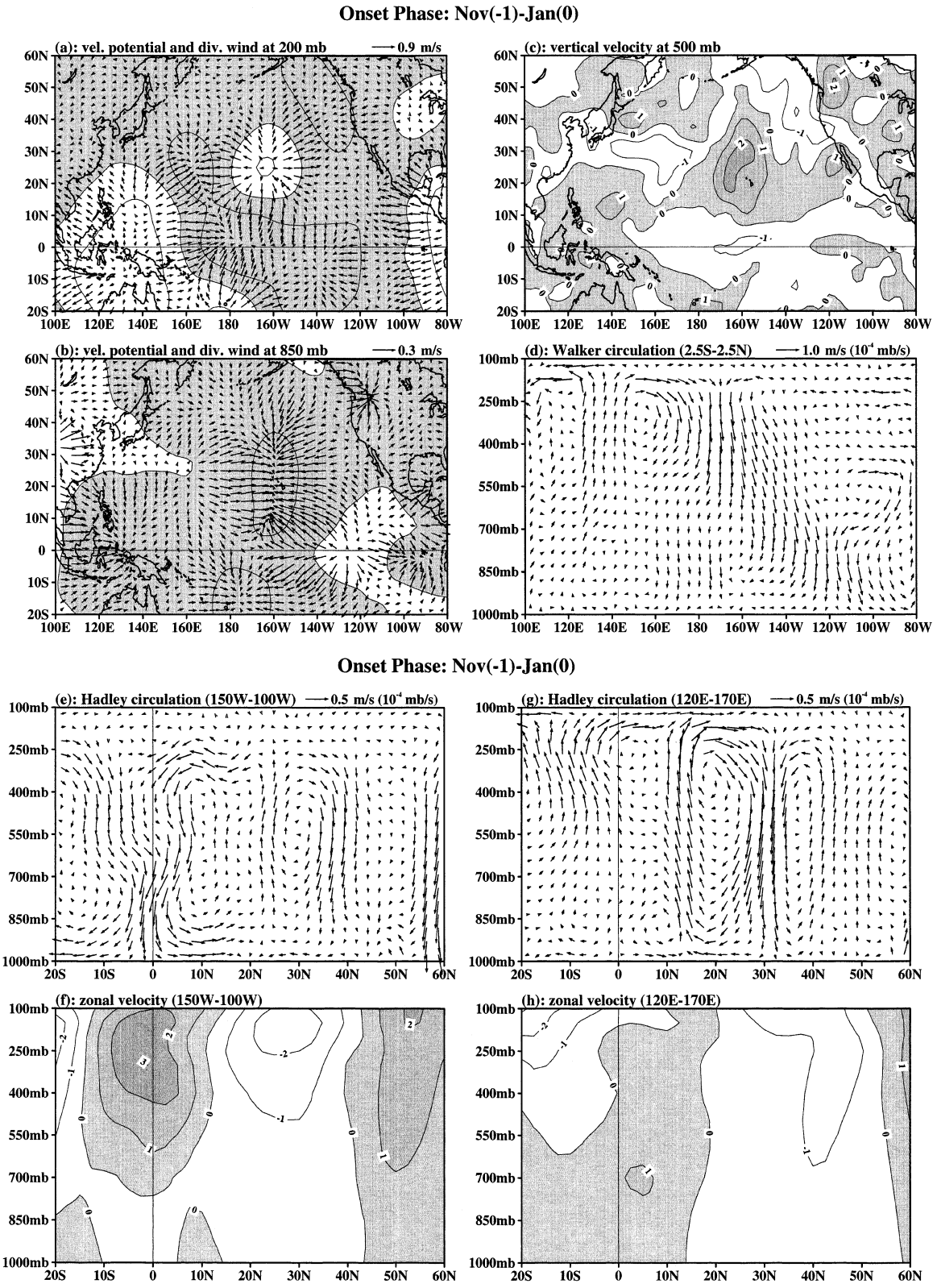

FIG. 7. As in Fig. 6, but during the onset phase of El Niño.

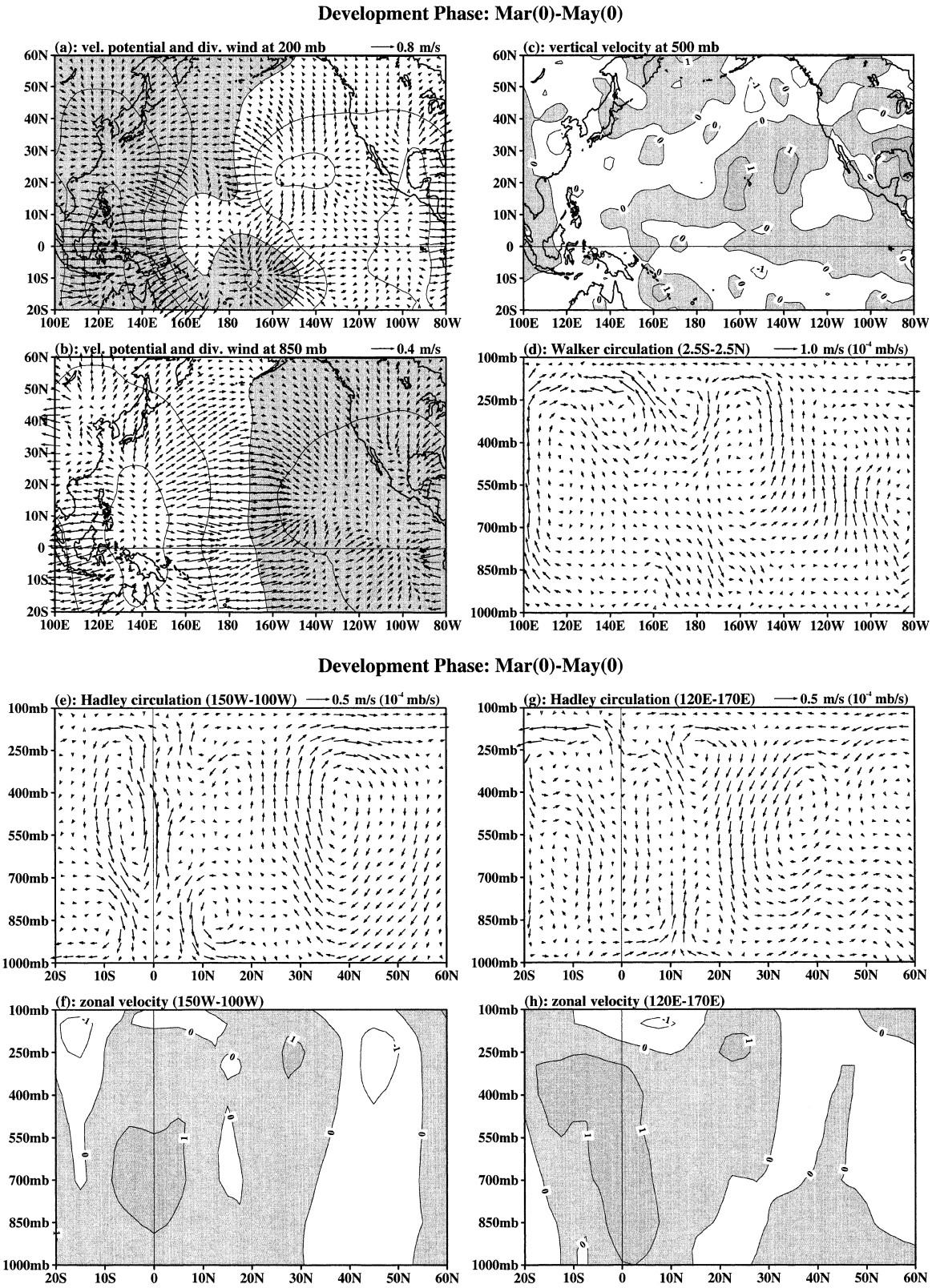

FIG. 8. As in Fig. 6, but during the development phase of El Niño.

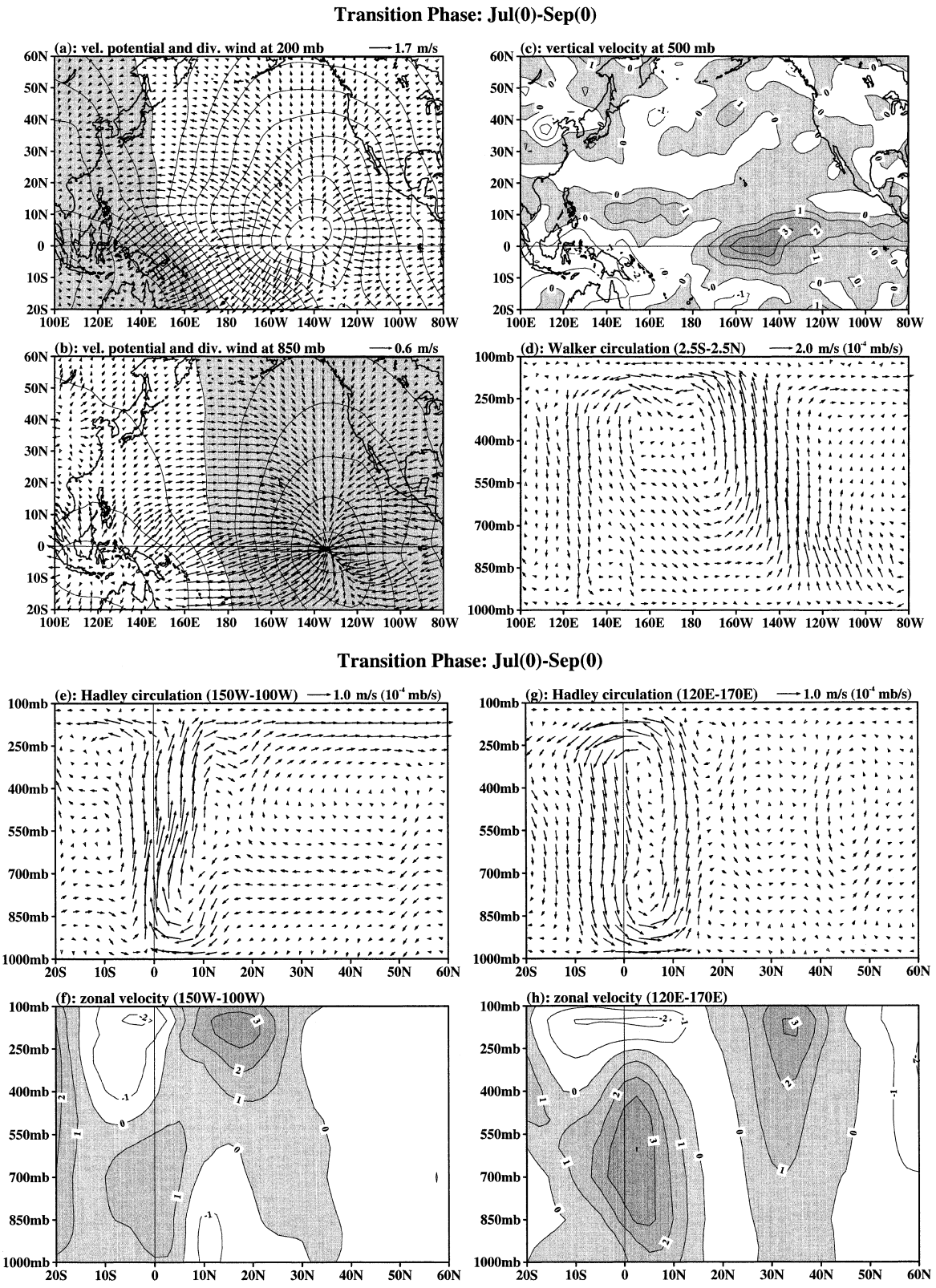

FIG. 9. As in Fig. 6, but during the transition phase of El Niño.

western Pacific continue to develop and in both the west and east, upper-tropospheric equatorial easterly wind anomalies are further strengthened (Figs. 9f and 9h). In the midlatitudes, westerly wind anomalies are centered in the upper troposphere just below the tropopause.

In the mature phase (Fig. 5e), the equatorial eastern Pacific shows maximum anomalous warming, whereas the off-equatorial western Pacific and the central North Pacific show cold SST anomalies. Warm SST anomalies begin to develop along the east coast of Asia and the west coast of North America. During that time, upper-tropospheric velocity potential anomalies show two additional centers: one with divergent outflow near Mexico and the other with convergent inflow near 35°N, 170°E (Fig. 10a). This pattern is consistent with that of Mestas-Nuñez and Enfield (2001) who obtained an ENSO pattern based on positive minus negative phases of a global ENSO reconstruction of the Niño-3 SST anomaly index. Associated with these midlatitudinal divergent/convergent fields are midtropospheric anomalous descending motions in the central North Pacific and anomalous ascending motions near the east coast of Asia and the west coast of North America (Fig. 10c). The equatorial eastern Pacific shows anomalous ascending motion, whereas the tropical western Pacific displays maximum anomalous descending motions in the off-equatorial western Pacific. This distribution of midtropospheric vertical velocity anomalies is consistent with the ENSO western Pacific anomaly patterns identified previously in surface oceanic and atmospheric variables (Wang et al. 1999; Wang 2000). The zonal Walker and meridional Hadley circulation cells are now fully developed during that time (Figs. 10d, 10e, and 10g). In the eastern Pacific, lower-tropospheric equatorial westerly wind anomalies and upper-tropospheric equatorial easterly wind anomalies, and upper-tropospheric midlatitudinal westerly anomalies are fully strengthened (Fig. 10f). This wind distribution is consistent with the 200-mb wind composite of Arkin (1982) who suggested a pair of anomalous anticyclones straddling the equator during the mature phase of El Niño. Interestingly, an easterly wind anomaly jet appears in the upper troposphere along 50°N. In the western Pacific, upper- and lower-tropospheric equatorial winds have now switched to westerly and easterly wind anomalies, respectively (Fig. 10h). The switch (to equatorial easterly wind anomalies) of lower-tropospheric wind anomalies in the western Pacific is important to the evolution of ENSO since they can force eastward-propagating upwelling Kelvin waves that help terminate El Niño (e.g., Tang and Weisberg 1984; Philander 1985). The western Pacific also shows an easterly (westerly) wind anomaly jet located just below the tropospause along 30°(50°N).

With the formation of lower-tropospheric equatorial easterly wind anomalies over the western Pacific, warm SST anomalies in the equatorial eastern Pacific begin to decay, whereas the cold SST anomalies in the central North Pacific and the warm SST anomalies along the east coast of Asia and the west coast of North America continue to develop (Fig. 5f). During the decay phase, atmospheric cells are similar to those in the mature phase but with weak amplitudes. Lower-tropospheric equatorial easterly wind anomalies over the western Pacific are further increased (Fig. 11h) and the equatorial westerly wind anomaly jet of the lower troposphere over the eastern Pacific is further strengthened (Fig. 11f).

Anomalous MZC for the onset and mature phases of El Niño are shown in Figs. 12a and 12b, respectively. Associated with the central North Pacific warming during the onset phase (Fig. 5b), Fig. 12a shows anomalous ascending motion around 160°W and anomalous descending motion west of the date line. Since North Pacific SST anomalies during the mature phase reverse to cold anomalies from warm anomalies (Fig. 5e), the anomalous MZC also reverses sign (Fig. 12b). Associated with cold SST anomalies in the central North Pacific and warm SST anomalies in the east coast of Asia and the west coast of North America during the mature phase, Fig. 12b shows the air anomalously sinking in the central North Pacific, flowing westward and eastward in the lower troposphere, rising in the east coast of Asia and in the west coast of North America, and then returning back to the central North Pacific aloft. Recalling the annual cycle of the MZC (Fig. 3a), we see that the MZC is weakened during the mature phase of El Niño.

5. Temporal variations of anomalous circulation cells

In the previous section, we showed atmospheric circulation composites for the six different phases of El Niño. Next, we consider whether or not these atmospheric circulation patterns are evident in every warm event over the period of record. The time series for evolution of the Walker and Hadley circulation cells are first calculated. Consistent with composites in section 4, we calculate the 500-mb vertical velocity anomaly difference between the equatorial eastern Pacific (5°S–5°N, 160°–120°W) and the equatorial western Pacific (5°S–5°N, 120°–160°E) as an index of the Walker circulation, the 500-mb vertical velocity anomaly difference between the central North Pacific (25°–35°N, 170°E–150°W) and the equatorial eastern Pacific (5°S–5°N, 160°–120°W) as an index of the Hadley circulation in the eastern Pacific, and the 500-mb vertical velocity anomaly difference between the western North Pacific (25°–35°N, 110°–150°E) and the equatorial western Pacific (5°S–5°N, 120°–160°E) as an index of the Hadley circulation in the western Pacific. These indices are compared with the Niño-3 SST anomalies, as shown in Fig. 13. Both the Walker and Hadley circulation cells are evident in every El Niño–La Niña event. The maximum correlations of the Walker circulation and the eastern Pacific Hadley circulation with the Niño-3 SST anomalies are -0.79 and 0.75, respectively at zero lag

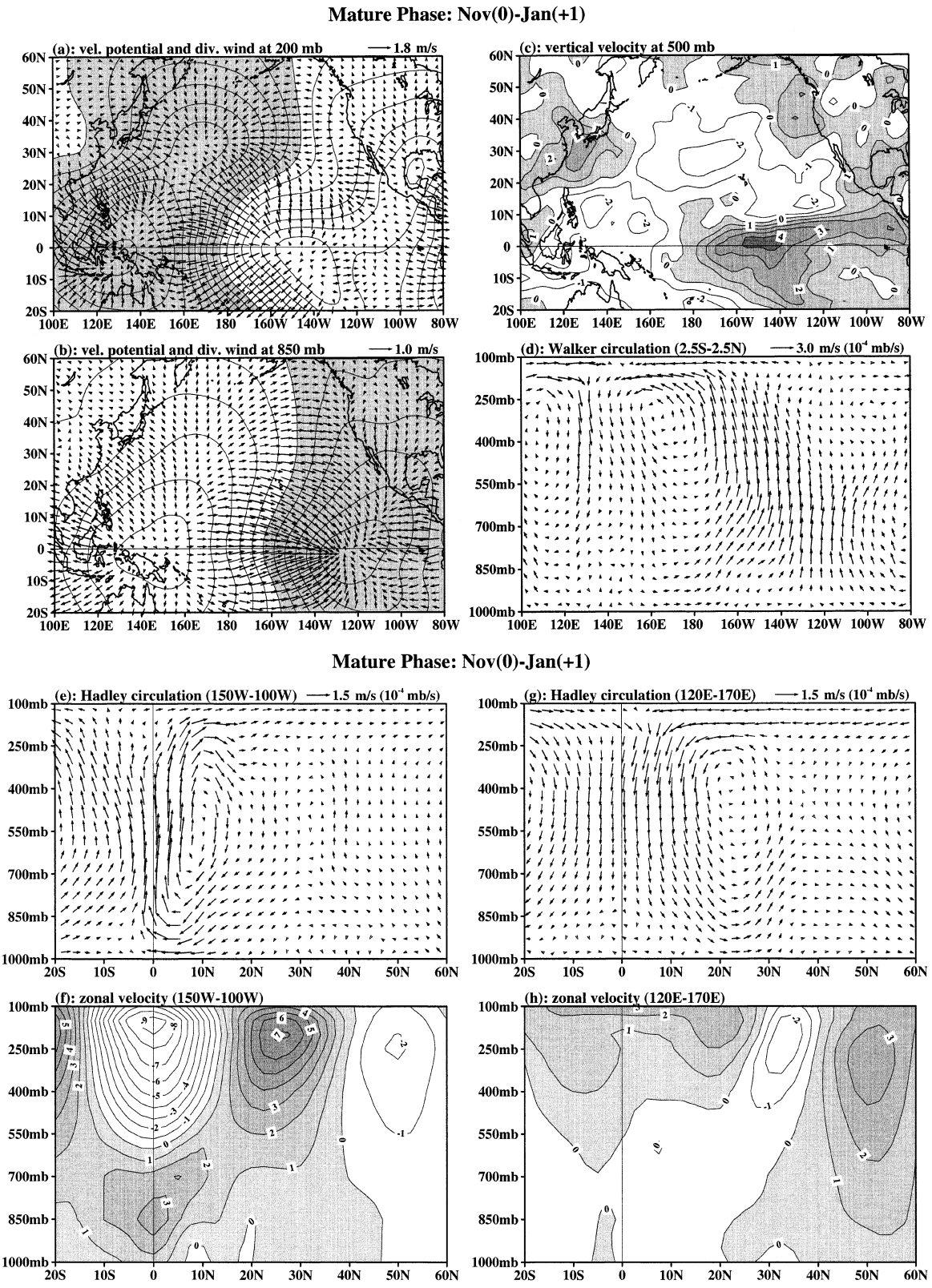

FIG. 10. As in Fig. 6, but during the mature phase of El Niño.

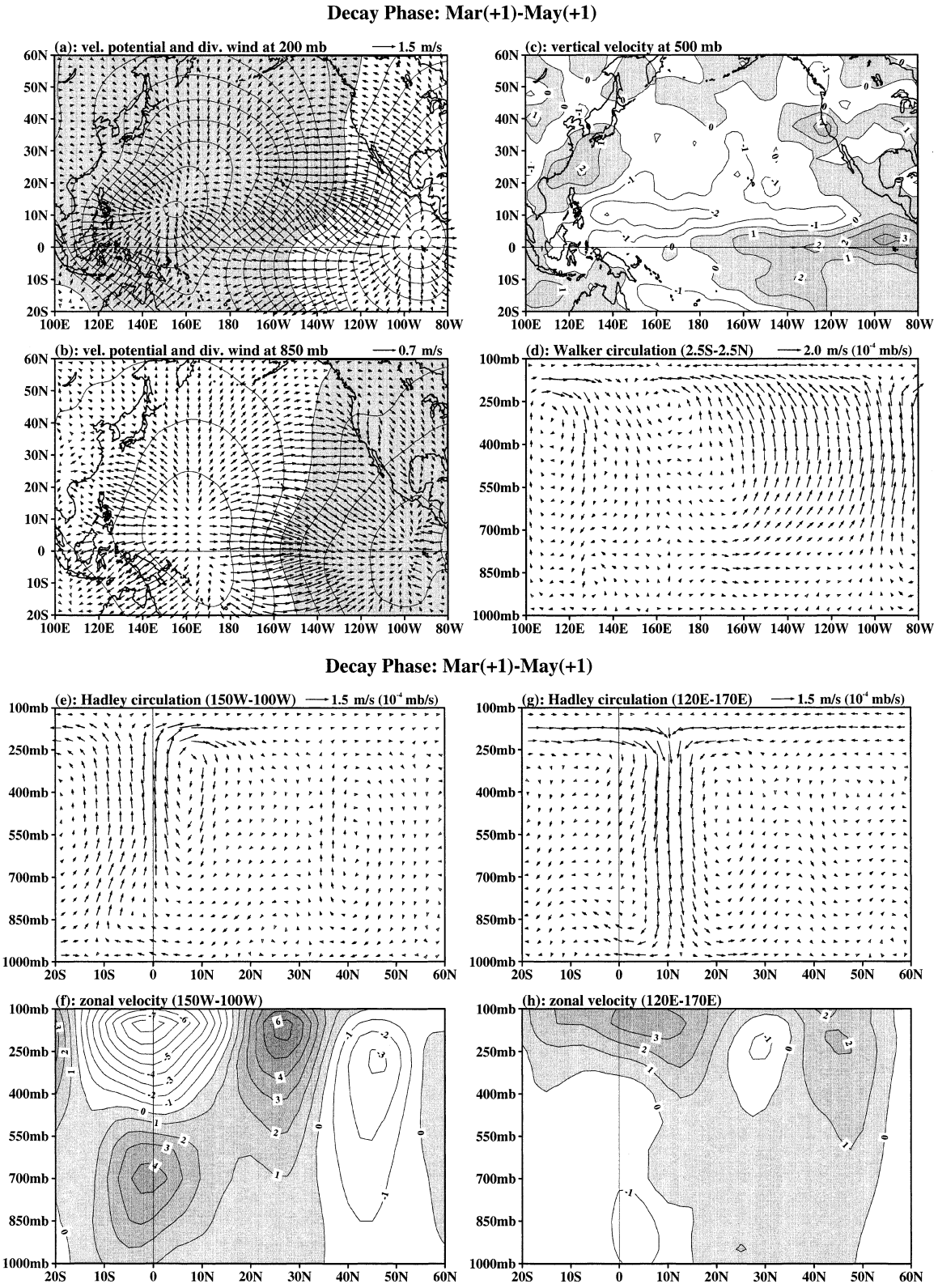

FIG. 11. As in Fig. 6, but during the decay phase of El Niño.

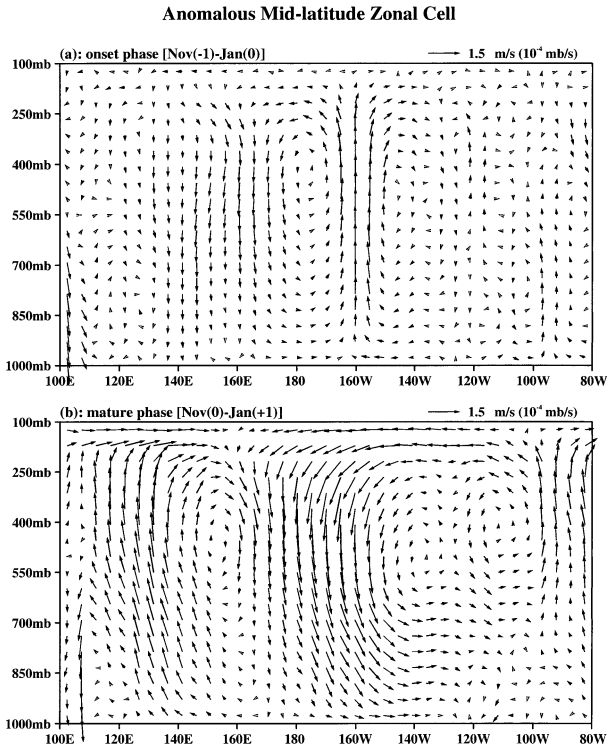

FIG. 12. Anomalous MZC for (a) the onset phase of El Niño and (b) the mature phase of El Niño. The divergent wind anomalies and vertical velocity anomalies are averaged between 27.5° and 32.5°N.

and are significant at the 99% level. For the western Pacific Hadley circulation, the maximum correlation is −0.56, with the Niño-3 SST anomalies leading the Hadley index by 2 months.

To measure the anomalous MZC, we calculate the time series of the 500-mb vertical velocity anomaly difference between the regions of the western North Pacific (25°–35°N, 110°–150°E) and the central North Pacific (25°–35°N, 170°E–150°W). The anomalous MZC index is compared with the Niño-3 SST anomalies, as shown in Fig. 14. When the equatorial eastern Pacific is warm, the MZC is weakened. The maximum correlation of −0.46 (above 99% significant level) occurs when the Niño-3 SST anomalies lead the MZC index by 2 months. Also shown is that the duration of the anomalous MZC is shorter than that of El Niño. The reason for this may be due to ENSO teleconnections (to the midlatitudes) that occur primarily during the NH winter (Horel and Wallace 1981), whereas El Niño warm events last at least one year.

The zonal wind anomaly composites in Figs. 6–11 show a significant lower-tropospheric variation in both the equatorial western and eastern Pacific. The indices of the 850-mb zonal wind anomalies in the equatorial western Pacific (5°S–5°N, 120°–170°E) and in the equatorial eastern Pacific (5°S–5°N, 150°–100°W) are shown in Figs. 15a and 15b, respectively. The maximum correlation of 0.56 occurs when the western Pacific zonal wind anomalies lead the Niño-3 SST anomalies by 4 months, whereas the maximum correlation between the eastern Pacific zonal wind anomalies and the Niño-3 SST anomalies is 0.67 at the zero month lag. The leading relationship between the western Pacific wind anomalies and the Niño-3 SST anomalies suggests that the western Pacific is an important region for initializing El Niño (e.g., Wang and Weisberg 2000; Wang 2001). The zonal wind anomaly composites (e.g., Fig. 10f) also display a strong ENSO signal in the upper troposphere of the equatorial eastern Pacific. In Fig. 15c, the 200-mb zonal wind anomalies in the equatorial eastern Pacific (5°S–5°N, 150°–100°W) are compared with the Niño-3 SST anomalies. When the equatorial eastern Pacific is warm (cold), the upper troposphere of the equatorial eastern Pacific is associated with easterly (westerly) wind anomalies. The calculation shows that the maximum correlation of −0.72 occurs when the Niño-3 SST anomalies lead the upper-tropospheric wind by 2 months.

During El Niño–La Niña events, the atmospheric westerly jet stream tends to move meridionally. The composite of Fig. 10f suggests that the jet stream may be measured by an index of the 200-mb zonal wind anomalies in the region of the eastern North Pacific (20°–30°N, 150°–100°W). Figure 16 compares the jet stream index with the Niño-3 SST anomalies. The maximum correlation of 0.70 occurs when the Niño-3 SST anomalies lead the jet stream index by 2 months. El Niño (La Niña) corresponds to westerly (easterly) wind anomalies in the upper troposphere of the midlatitude Pacific, associated with the equatorward (poleward) displacement of the jet stream.

6. Discussion and summary

Using the recently available atmospheric and oceanic data, the present paper describes and examines the seasonal and interannual variability of the atmospheric circulation over the Pacific where the largest of three major tropical heat sources is located (tropical western Pacific heat source). The others reside over the Amazon and Africa and are associated with Atlantic climate variability, which is discussed in a companion paper (Wang 2002, manuscript submitted to *J. Climate*). The tropical western Pacific heat source is farthest north and west in the boreal summer, and farthest south and east in the boreal winter. Associated with this seasonal movement of the heat source are seasonal variations of the equatorial zonal Walker cell, the tropical meridional Hadley cell, the extratropical meridional Ferrel cell, and the extratropical zonal MZC. The jet stream is strong and southernmost in the boreal winter, whereas it weakens and moves northward during the boreal summer.

Based on the data presented in this study, the mean state and anomaly of the equatorial zonal Walker cell, the tropical meridional Hadley cell, the extratropical meridional Ferrel cell, and the extratropical zonal MZC are summarized in Fig. 17. Unlike in the western Pacific

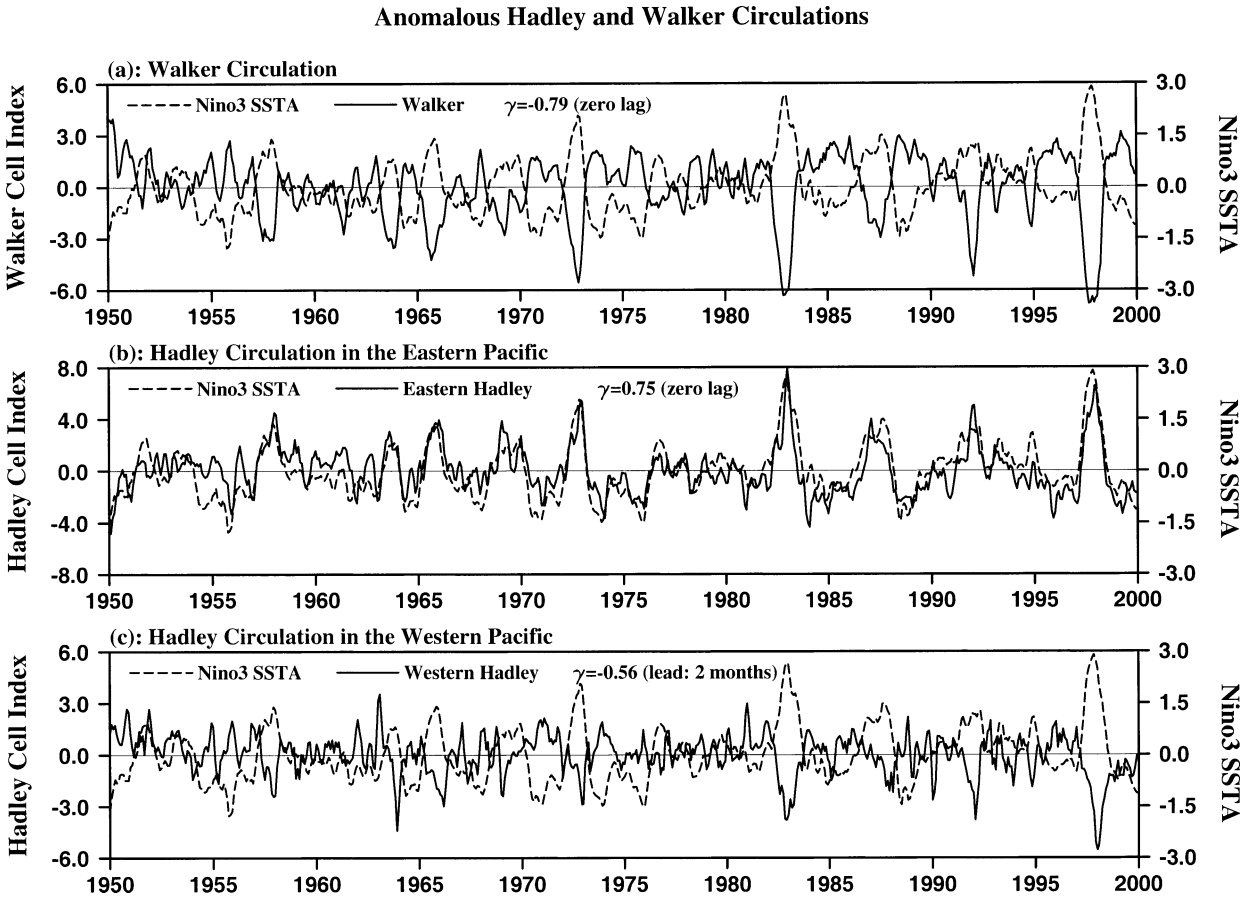

FIG. 13. Comparison of the Niño-3 SST anomalies with (a) the Walker cell index, (b) the eastern Pacific Hadley cell index, and (c) the western Pacific Hadley cell index. The Walker cell index is defined by 500-mb vertical velocity anomaly difference between the equatorial eastern Pacific (5°S–5°N, 160°–120°W) and the equatorial western Pacific (5°S–5°N, 120°–160°E). The eastern Pacific Hadley cell index is defined by 500-mb vertical velocity anomaly difference between the central North Pacific (25°–35°N, 170°E–150°W) and the equatorial eastern Pacific (5°S–5°N, 160°–120°W). The western Pacific Hadley index is defined by 500-mb vertical velocity anomaly difference between the western North Pacific (25°–35°N, 110°–150°E) and the equatorial western Pacific (5°S–5°N, 120°–160°E). All of the time series are 3-month running means. The γ represents the correlation coefficient.

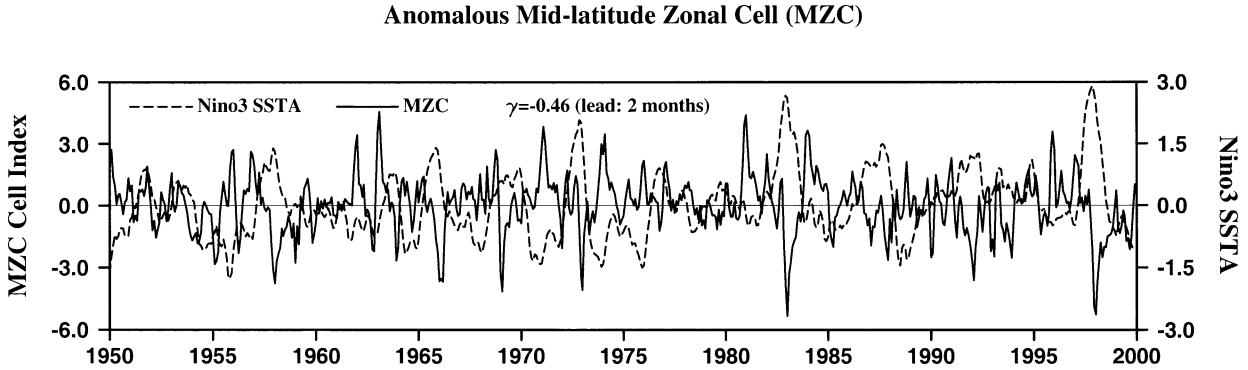

FIG. 14. Comparison of the Niño-3 SST anomalies with the MZC index. The MZC index is defined by 500-mb vertical velocity anomaly difference between the western North Pacific (25°–35°N, 110°–150°E) and the central North Pacific (25°–35°N, 170°E–150°W). All of the time series are 3-month running means. The γ represents the correlation coefficient.

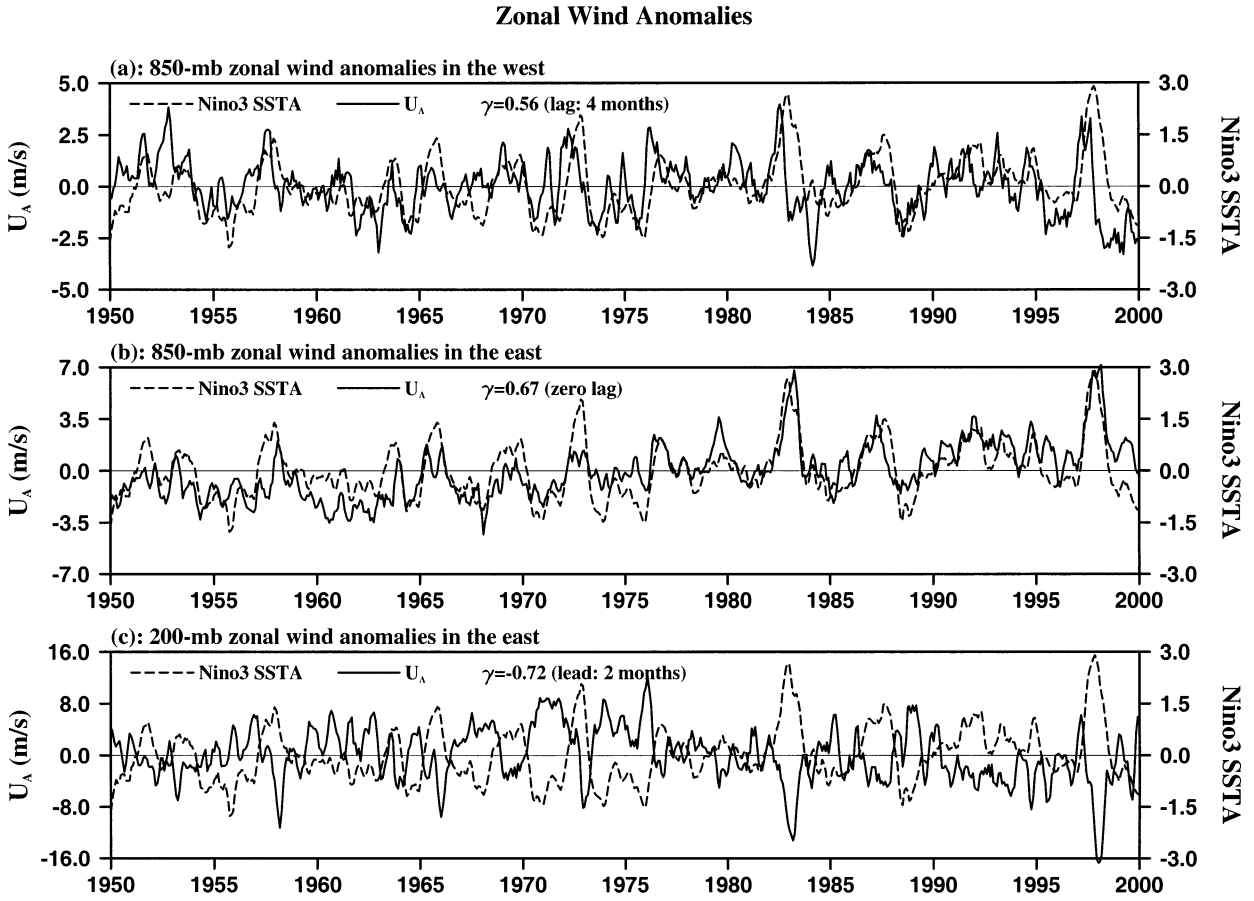

FIG. 15. Comparison of the Niño-3 SST anomalies with (a) 850-mb zonal wind anomalies in the equatorial western Pacific (5°S–5°N, 120°–170°E); (b) 850-mb zonal wind anomalies in the equatorial eastern Pacific (5°S–5°N, 150°–100°W); (c) 200-mb zonal wind anomalies in the equatorial eastern Pacific (5°S–5°N, 150°–100°W). All of the time series are 3-month running means. The γ represents the correlation coefficient.

that shows a single Hadley cell, the mean meridional circulation in the eastern Pacific shows three cells: two Hadley cells and one Ferrel cell. The tropical north and south Hadley cells are characterized by the air rising in the ITCZ, diverging northward and southward in the upper troposphere, and descending over the regions of the subtropical high and the equatorial eastern Pacific cold tongue. The atmospheric cells vary with the interannual phenomenon of ENSO. During the mature phase of El Niño, both the Walker circulation cell and the MZC

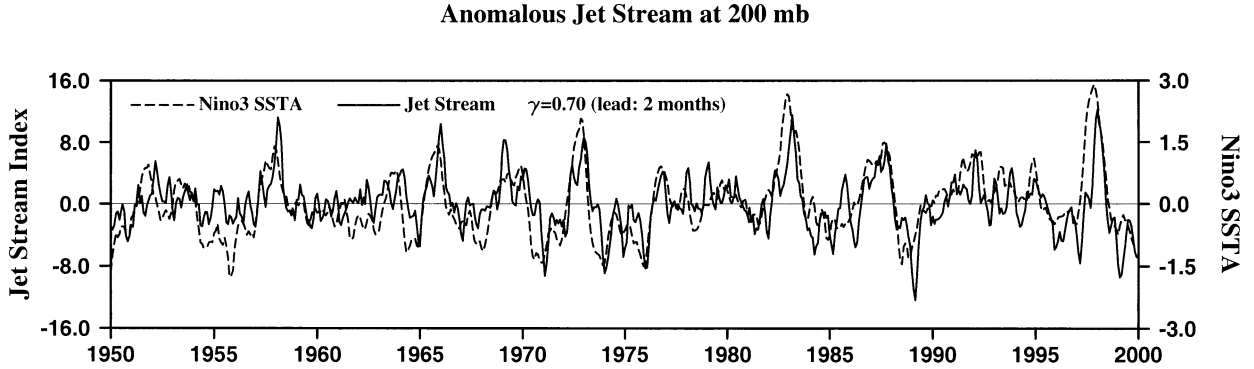

FIG. 16. Comparison of the Niño-3 SST anomalies with the jet stream index. The jet stream index is defined by 200-mb zonal wind anomalies in the eastern North Pacific (20°–30°N, 150°–100°W). All of the time series are 3-month running means. The γ represents the correlation coefficient.

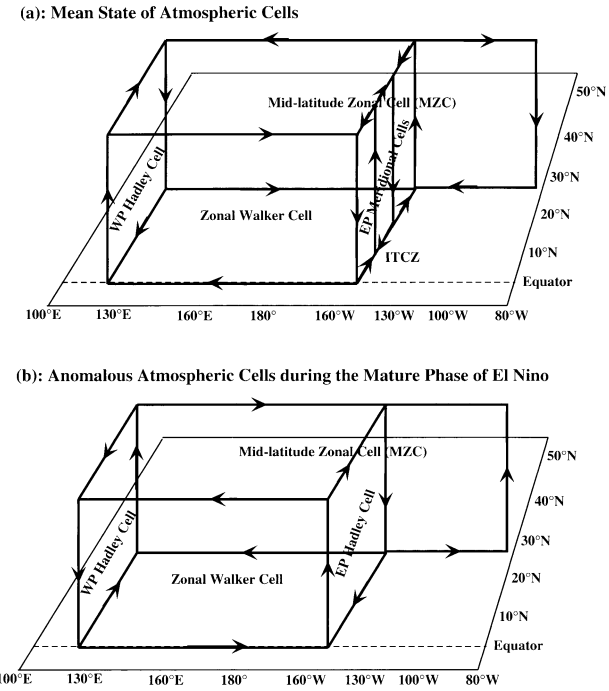

FIG. 17. Schematic diagrams summarized (a) mean state of atmospheric circulation cells and (b) anomalous atmospheric cells during the mature phase of El Niño. Shown are the equatorial zonal Walker cell, the merdional Hadley cell in the western Pacific (WP), the meridional Hadley and Ferrel cells in the eastern Pacific (EP), and the MZC. The schematic diagrams are drawn, based on the data presented in this study.

are weakened. The anomalous Hadley cell in the eastern Pacific during the mature phase of El Niño shows the air rising in the tropical region, flowing northward in the upper troposphere, descending in the midlatitude, and returning to the Tropics in the lower troposphere. The anomalous Hadley cell in the western Pacific has an opposite rotation as that of the anomalous Hadley cell in the eastern Pacific.

Since the pioneering work of Bjerknes (1966 and 1969), ENSO has been recognized as an interannual phenomenon involved ocean–atmosphere interactions associated with the Pacific Walker circulation (e.g., Philander 1990; Neelin et al. 1998). The data-derived variation of the Walker circulation shows that interannual east–west motion of the Walker circulation cell, associated with large changes in atmospheric convection, plays an important role in the evolution of ENSO. During El Niño (SST is warming in the equatorial eastern and central Pacific), the tropical western Pacific heat source associated with lower-tropospheric convergence, upper-tropospheric divergence, and midtropospheric ascending motion, moves eastward. This eastward movement weakens the Walker circulation cell that then weakens the lower-tropospheric equatorial easterly trade winds (the low branch of east–west air exchange in the Walker cell) and thus further increases SST in the equatorial eastern and central Pacific. This positive ocean–atmosphere feedback associated with the zonal Pacific Walker circulation cell is a key for the development of the Pacific El Niño.

The anomalous Hadley circulation cells in the eastern Pacific and in the western Pacific behave oppositely. During El Niño, the eastern (western) Pacific Hadley cell shows a clockwise (counterclockwise) rotation with anomalous ascending (descending) motion in the Tropics and anomalous descending (ascending) motion in the subtropics. This is consistent with SST-related heating that is a driving force for the Hadley circulation (e.g., Holton 1992). El Niño shows positive SST anomalies in the equatorial eastern Pacific and negative SST anomalies in the tropical western Pacific. Corresponding to this SST anomaly distribution are lower-tropospheric anomalous convergence (divergence), upper-tropospheric anomalous divergence (convergence), and midtropospheric anomalous ascending (descending) motion in the tropical eastern (western) Pacific. Thus, the anomalous eastern (western) Pacific Hadley cell shows the air rising (sinking) in the Tropics, flowing poleward (equatorward) in the upper troposphere, sinking (rising) in the subtropics, and flowing equatorward (poleward) in the lower troposphere.

The Hadley circulation is originally referred to a global zonal mean meridional circulation (e.g., Oort and Yienger 1996; Trenberth et al. 2000; and references therein), whereas the meridional circulation in this study is regional. Since ENSO is characterized as a strong east–west contrast phenomenon, a global zonal mean may have shortcomings. For example, Oort and Yienger (1996) calculated the global zonal mean streamfunction by using the zonal mean meridional wind component from 1964 to 1989. They chose the maximum streamfunction in the Tropics as a measure of the strength of the Hadley circulation. Based on their calculations, they concluded a positive correlation relationship between the Hadley cell and ENSO. However, the 1982/83 El Niño is not consistent with their conclusion. This may be simply due to the strong east–west asymmetry associated with ENSO. Our analysis shows that the anomalous Hadlley cells in the eastern and western Pacific have opposite signs.

In comparison with the anomalous Hadley circulation cell, the anomalous Ferrel circulation cell associated with ENSO is weak and is not well organized. The reason for this may be due to different driving mechanisms for the Hadley and Ferrel cells. The tropical Hadley cell is a thermally driven cell, whereas the extratropical Ferrel cell is an indirectly thermally driven cell. The Hadley cell is forced by diabatic heating, but the Ferrel cell is forced mostly by transient baroclinic eddy activity through associated poleward heat and momentum transports (e.g., Holton 1992). Since El Niño is associated with tropical SST-related heating, the tropical Hadley cell is thus clearly shown up during El Niño.

The divergent wind and vertical motion of the NCEP–NCAR reanalysis field show the MZC in the North Pa-

cific. The mean MZC is characterized by the air rising in the central North Pacific, diverging westward and eastward in the upper troposphere, descending over the regions of the east coast of Asia and the west coast of North America, then flowing back to the central North Pacific in the lower troposphere. The MZC is strong and easternmost in the boreal winter. The MZC also varies with El Niño, showing a weakening of the MZC during the mature phase of El Niño. Since the main impact of El Niño to the extratropics is likely to be felt during the winter months (Horel and Wallace 1981), the duration of the MZC is observed to be shorter than that of El Niño. In addition, we should keep in mind that, like the Walker and Hadley cells, the MZC in this paper is identified by the divergent wind and the pressure vertical velocity. If we also consider the rotational wind (e.g., see Figs. 1f and 1h), the MZC is not a closed cell.

Earlier ENSO studies mainly focused on the ENSO eastern Pacific anomaly patterns (e.g., Rasmusson and Carpenter 1982), probably because interannual anomalies are large in the eastern/central Pacific and ENSO is developed from the far eastern Pacific for the events before the 1980s. Recently, Wang et al. (1999) and Wang and Weisberg (2000) emphasized the western Pacific anomaly patterns in addition to the eastern Pacific anomaly patterns. During the warm phase of ENSO, warm SST and low sea level pressure (SLP) anomalies in the equatorial eastern Pacific and low outgoing longwave radiation (OLR) anomalies in the equatorial central Pacific are accompanied by cold SST and high SLP anomalies in the off-equatorial western Pacific and high OLR anomalies in the off-equatorial far western Pacific. Also, while the surface zonal wind anomalies over the equatorial central Pacific are westerly, those over the equatorial western Pacific are easterly. The present analysis shows that the western Pacific patterns are also manifested in the troposphere. The mature phase of El Niño shows anomalous ascending motion in the equatorial eastern Pacific and anomalous descending motion in the off-equatorial western Pacific. The western Pacific anomaly patterns are robust features of ENSO and are independent of datasets. Herein, our analyses also point out how important the western Pacific is in the evolution of ENSO. The lower-tropospheric wind anomalies in the equatorial western Pacific are significantly correlated with the Niño-3 SST anomalies, with western Pacific wind anomalies leading the Niño-3 SST anomalies by 4 months. This suggests that the western Pacific is an important region for initiating and terminating El Niño. This is also consistent with the unified ENSO oscillator (Wang 2001) that suggests that the ENSO mechanisms of the delayed oscillator (Suarez and Schopf 1988; Battisti and Hirst 1989), the western Pacific oscillator (Weisberg and Wang 1997; Wang et al. 1999), the recharge–discharge oscillator (Jin 1997), and the advective–reflective oscillator (Picaut et al. 1997) may all be operated.

Acknowledgments. This work was supported by a grant from the National Oceanic and Atmospheric Administration (NOAA) Office of Global Programs (CLIVAR-Pacific), by a grant from the NASA Seasonal-to-Interannual Prediction Project (NSIPP), and by the base funding of the NOAA Atlantic Oceanographic and Meteorological Laboratory. Comments by R. Molinari, D. Enfield, D. Mayer, and two anonymous reviewers helped to improve the manuscript. Discussions with T. N. Krishnamurti and C. Rooth are appreciated. J. Harris assisted with the initial processing of the NCEP–NCAR reanalysis field.

REFERENCES

Arkin, P. A., 1982: The relationship between interannual variability in the 200 mb tropical wind field and the Southern Oscillation. *Mon. Wea. Rev.*, **110,** 1393–1404.

Battisti, D. S., and A. C. Hirst, 1989: Interannual variability in a tropical atmosphere–ocean model: Influence of the basic state, ocean geometry and nonlineary. *J. Atmos. Sci.,* **46,** 1687–1712.

Bjerknes, J., 1966: A possible response of the atmospheric Hadley circulation to equatorial anomalies of ocean temperature. *Tellus,* **18,** 820–829.

——, 1969: Atmospheric teleconnections from the equatorial Pacific. *Mon. Wea. Rev.,* **97,** 163–172.

Busalacchi, A., and J. J. O'Brien, 1981: Interannual variability of the equatorial Pacific in the 1960s. *J. Geophys. Res.,* **86,** 10 901–10 907.

Hastenrath, S., 2001: In search of zonal circulations in the equatorial Atlantic sector from the NCEP–NCAR reanalysis. *Int. J. Climatol.,* **21,** 37–47.

Holton, J. R., 1992: *An Introduction to Dynamic Meteorology.* 3d ed. Academic Press, 511 pp.

Horel, J. D., and J. M. Wallace, 1981: Planetary-scale atmospheric phenomena associated with the Southern Oscillation. *Mon. Wea. Rev.,* **109,** 813–829.

Jin, F. F., 1997: An equatorial ocean recharge paradigm for ENSO. Part I: Conceptual model. *J. Atmos. Sci.,* **54,** 811–829.

Kalnay, E., and Coauthors, 1996: The NCEP/NCAR 40-Year Reanalysis Project. *Bull. Amer. Meteor. Soc.,* **77,** 437–471.

Krishnamurti, T. N., 1971: Tropical east–west circulations during the northern summer. *J. Atmos. Sci.,* **28,** 1342–1347.

——, M. Kanamitsu, W. J. Koss, and J. D. Lee, 1973: Tropical east–west circulations during the northern winter. *J. Atmos. Sci.,* **30,** 780–787.

Mancuso, R. L., 1967: A numerical procedure for computing fields of streamfunction and velocity potential. *J. Appl. Meteor.,* **6,** 994–1001.

McCreary, J. P., 1976: Eastern tropical ocean response to changing wind systems: With applications to El Niño. *J. Phys. Oceanogr.,* **6,** 632–645.

——, and D. L. T. Anderson, 1991: An overview of coupled ocean–atmosphere models of El Niño and the Southern Oscillation. *J. Geophys. Res.,* **96,** 3125–3150.

McPhaden, M. J., and Coauthors, 1998: The Tropical Ocean–Global Atmosphere observing system: A decade of progress. *J. Geophys. Res.,* **103,** 14 169–14 240.

Mestas-Nuñez, A. M., and D. B. Enfield, 2001: Eastern equatorial Pacific SST variability: ENSO and non-ENSO components and their climatic associations. *J. Climate,* **14,** 391–402.

Neelin, J. D., D. S. Battisti, A. C. Hirst, F.-F. Jin, Y. Wakata, T. Yamagata, and S. E. Zebiak, 1998: ENSO theory. *J. Geophys. Res.,* **103,** 14 262–14 290.

Newman, M., P. D. Sardeshmukh, and J. W. Bergman, 2000: An assessment of the NCEP, NASA, and ECMWF reanalyses over

the tropical west Pacific warm pool. *Bull. Amer. Meteor. Soc.,* **81,** 41–48.
Oort, A. H., and J. J. Yienger, 1996: Observed interannual variability in the Hadley Circulation and its connection to ENSO. *J. Climate,* **9,** 2751–2767.
Philander, S. G., 1981: The response of equatorial oceans to a relaxation of the trade winds. *J. Phys. Oceanogr.,* **11,** 176–189.
——, 1985: El Niño and La Niña. *J. Atmos. Sci.,* **42,** 2652–2662.
——, 1990: *El Niño, La Niña, and the Southern Oscillation.* Academic Press, 289 pp.
Picaut, J., F. Masia, and Y. du Penhoat, 1997: An advective-reflective conceptual model for the oscillatory nature of the ENSO. *Science,* **277,** 663–666.
Rasmusson, E. M., and T. H. Carpenter, 1982: Variations in tropical sea surface temperature and surface wind fields associated with the Southern Oscillation/El Niño. *Mon. Wea. Rev.,* **110,** 354–384.
Smith, T. M., R. W. Reynolds, R. E. Livezey, and D. C. Stokes, 1996: Reconstruction of historical sea surface temperature using empirical orthogonal functions. *J. Climate,* **9,** 1403–1420.
Suarez, M. J., and P. S. Schopf, 1988: A delayed action oscillator for ENSO. *J. Atmos. Sci.,* **45,** 3283–3287.
Tang, T. Y., and R. H. Weisberg, 1984: On the equatorial Pacific response to the 1982/1983 El Niño–Southern Oscillation event. *J. Mar. Res.,* **42,** 809–829.
Trenberth, K. E., and D. P. Stepaniak, 2001: Indices of El Niño evolution. *J. Climate,* **14,** 1697–1701.
——, ——, and J. M. Caron, 2000: The global monsoon as seen through the divergent atmospheric circulation. *J. Climate,* **13,** 3969–3993.
Walker, G. T., 1923: Correlation in seasonal variations of weather VIII: A preliminary study of world weather. *Mem. Indian Meteor. Dept.,* **24,** 75–131.
——, 1924: Correlation in seasonal variations of weather IX: A further study of world weather. *Mem. Indian Meteor. Dept.,* **24,** 275–332.
——, 1928: World weather III. *Mem. Roy. Meteor. Soc.,* **2,** 97–106.
Wang, B., 1995: Interdecadal changes in El Niño onset in the last four decades. *J. Climate,* **8,** 267–285.
Wang, C., 2000: On the atmospheric responses to tropical Pacific heating during the mature phase of El Niño. *J. Atmos. Sci.,* **57,** 3767–3781.
——, 2001: A unified oscillator model for the El Niño–Southern Oscillation. *J. Climate,* **14,** 98–115.
——, and R. H. Weisberg, 2000: The 1997–98 El Niño evolution relative to previous El Niño events. *J. Climate,* **13,** 488–501.
——, ——, and J. I. Virmani, 1999: Western Pacific interannual variability associated with the El Niño–Southern Oscillation. *J. Geophys. Res.,* **104,** 5131–5149.
Webster, P. J., and H. R. Chang, 1988: Equatorial energy accumulation and emanation regions: Impacts of a zonally varying basic state. *J. Atmos. Sci.,* **45,** 803–829.
Weisberg, R. H., and C. Wang, 1997: A western Pacific oscillator paradigm for the El Niño–Southern Oscillation. *Geophys. Res. Lett.,* **24,** 779–782.
Wyrtki, K., 1975: El Niño—The dynamic response of the equatorial Pacific Ocean to atmospheric forcing. *J. Phys. Oceanogr.,* **5,** 572–584.